IEEE Access
Multidisciplinary | Rapid Review | Open Access Journal

Received September 3, 2019, accepted September 17, 2019, date of publication September 23, 2019,
date of current version October 4, 2019.

Digital Object Identifier 10.1109/ACCESS.2019.2942992

Performance of Decode-and-Forward Relaying in Mixed Beaulieu-Xie and $\mathcal{M}$ Dual-Hop Transmission Systems With Digital Coherent Detection

JIASHUN HU[1], ZAICHEN ZHANG[1,2], (Senior Member, IEEE), JIAN DANG[1], (Member, IEEE), LIANG WU[1], (Member, IEEE), AND GUANGHAO ZHU[3]

[1]National Mobile Communications Research Laboratory, Southeast University, Nanjing 210096, China
[2]Purple Mountain Laboratories, Nanjing 211111, China
[3]School of Electronic Science and Engineering, Nanjing University, Nanjing 210023, China

Corresponding author: Zaichen Zhang (zczhang@seu.edu.cn)

This work was supported in part by the National Key Research and Development Plan Projects under Grant 2016YFB0502202 and Grant 2016YFB0502202, in part by the NSFC Projects under Grant 61960206005, Grant 61571105, and Grant 61971136, in part by the Fundamental Research Funds for the Central Universities, and in part by the Zhishan Youth Scholar Program of SEU.

ABSTRACT Performance analysis is presented for a decode-and-forward protocol based mixed radio-frequency (RF) and free-space optical (FSO) dual-hop transmission system with digital coherent detection. The RF path is modeled by Beaulieu-Xie fading, while the FSO hop is characterised by the Málaga ($\mathcal{M}$) distributed turbulence with pointing errors. We first derive novel and exact analytical expressions for the cumulative distribution function (CDF), the probability density function and the moment generating function (MGF) of the overall signal-to-noise ratio by means of Meijer's G function, followed by the accurate infinite series expressions of the performance criterions, such as the outage probability, the average bit-error rate (BER) and the ergodic capacity (average channel capacity). Asymptotic analysis for the CDF, the MGF, the outage probability, the average BER, and the ergodic capacity is also provided. Monte Carlo simulations are performed to verify these derived expressions.

INDEX TERMS Mixed RF/FSO systems, digital coherent detection, Beaulieu-Xie fading, Málaga turbulence, decode-and-forward relaying.

I. INTRODUCTION

Free-space optical (FSO) communication, referring to optical signals transmission through the free space, has caught continuous attention owing to lower cost, better security, wider yet license-free bandwidth compared with radio-frequency (RF) solutions [1]. However, FSO communication systems are impaired by atmospheric effects, including attenuation, turbulence induced fading and pointing errors, which limit the transmission distance.

Cooperative relaying, which has been extensively used in RF wireless communication systems (e.g., the unmanned aerial vehicle relaying [2]), is one of efficient solutions proposed to broaden the coverage and mitigate the turbulence induced fading for FSO systems [3]. The amplify-and-forward (AF) and decode-and-forward (DF) relay, also known as nonregenerative and regenerative relay, are the two main relaying strategies used in the relay-assisted systems [4]. The relay in AF systems just amplifies and forwards the arriving signals, while the relay in DF systems fully decodes the received signals and retransmits the re-encoded version to the next hop [4]. Although the operation for the AF relay is simpler than that of the DF relay, its transceivers need expensive RF chains [5] and the additive noise is amplified as well. Besides, due to cost considerations, components with lower quality are often employed in relay nodes, e.g., the use of low power low-resolution analog-to-digital converters (ADCs) and digital-to-analog converters in massive multiple-input multiple-output relaying systems [6], but these components may be prone to impairments and

The associate editor coordinating the review of this manuscript and approving it for publication was Jiayi Zhang.

cause distortion [7]. The DF protocol has been proven to be more robust to hardware impairments in one-way relaying systems [8].

Considerable efforts have been devoted to evaluate the performance of AF and DF relaying strategies over FSO links [9]–[15]. Most of those studies focus on the symmetric relay systems, in which every relay link experiences the same channel fading. Nevertheless, the signals on each hop may be transmitted by various communication systems or go through different physical links in practical scenarios [16]. A mixed RF/FSO dual-hop transmission system was proposed in [16]. The system, combining the characteristics of RF and FSO, is considered to be more effective and adaptive in real communications networks [16], [17]. It also offers a promising solution to overcome the connectivity gap between the last-mile access and the optical backbone networks because many RF subscribers can be multiplexed through the FSO link [18]. Therefore, the performance of mixed RF/FSO systems have been extensively investigated [17]–[28].

In [16], the outage probability of the mixed Rayleigh and Gamma-Gamma dual-hop system with a fixed gain AF relay as well as the subcarrier intensity modulation (SIM) scheme was derived for the first time. Later, the average symbol error rate of the mixed Rayleigh and $\mathcal{M}$ dual-hop system employing both fixed gain and channel-dependent (variable gain) AF relay schemes was investigated in [21]. Particularly, by assuming the channel state information of the RF path was outdated, the authors in [18] analyzed the outage probability and the average bit-error rate (BER) of a mixed RF/FSO system with variable gain AF relaying, whose RF path was Rayleigh distributed and FSO link experienced Gamma-Gamma turbulence with pointing errors. However, the Rayleigh distribution cannot be used to represent the RF path consisting of a line-of-sight (LOS) component. In [20], the RF path was assumed to follow the Nakagami-m distribution, while the FSO link is assumed to experience Gamma-Gamma turbulence with pointing errors. The performance analysis was carried out with both intensity modulation with direct detection (IM/DD) and heterodyne detection schemes. Recently, the performance of a mixed millimeter-wave (mmWave) RF/FSO system has been studied in [26]. The mmWave RF channel was modeled by the Rician distribution and the FSO channel was modeled by $\mathcal{M}$ turbulence with pointing errors. However, the RF paths in these studies are described to follow the Rayleigh, Nakagami-m, and Ricean distributions. Besides the inconsistency between the tail and the experimental data [24], the Nakagami-m and Rayleigh distributions may fail to catch the fading statistics of future femtocell channels with diffusing multipath components and many direct LOS components [29], [30]. The generalized Ricean distribution is able to describe a LOS component and diffuse scatter components, but its fading severity parameter is simple and less flexible [29]. A novel fading model (which is referred to as Beaulieu-Xie fading model [31]), representing both diffuse scatter and LOS components, has been proposed by introducing a special scale to non-central chi-distribution distributed variables [29]. The new model uses the same definition of the fading figure m as the Nakagami-m distribution, which makes the model has the flexibility in adjusting the severity of the fading [29]. Moreover, it provides a unified framework for generalized Ricean, non-central chi and $\kappa - \mu$ distributions [29]. There are many atmospheric turbulence models in the current literature as well. The $\mathcal{M}$ turbulence, which is also a generalized statistical model, unifies most of widely accepted atmospheric turbulence models, e.g., the Gamma-Gamma, the lognormal, and the K models [32]. Furthermore, it is in good agreement with published simulation data under varying turbulence conditions [32].

Owing to low cost and easy implementation, on-off keying (OOK) with IM/DD is usually the first modulation/detection choice for FSO systems. However, it is very difficult for an OOK IM/DD system to obtain the optimal error rate performance with a fixed detection threshold because of the atmospheric turbulence fading [33]. Coherent detection (CD) and subcarrier phase-shift keying (PSK) have been introduced to solve the threshold problem in OOK IM/DD systems [33]. Compared with the SIM system, the coherent FSO system can further achieve 24-30 dB improvements in sensitivity [34]. Coherent systems can be classified into carrier-phase sensitive and carrier-phase insensitive systems based on whether carrier-phase recovery must be done at the optical stage [35]. Carrier-phase sensitive systems, also known as optical phase-locked loop (OPLL)-based homodyne detection systems, can get the baseband signal directly [35]. However, it is difficult to lock the carrier phase drift stably [35]. Carrier-phase insensitive systems can be further divided into heterodyne detection and phase-diversity homodyne detection systems according to the receivers that they used [35]. The heterodyne receiver needs to deal with an intermediate frequency (IF) to obtain the baseband signal, and the IF should be much higher than the bit rate of the system [35]. Recent developments in high-speed and real-time digital signal processing (DSP) made the carrier phase could be estimated via simple and efficient DSP algorithms after phase-diversity homodyne detection [35]. Therefore, digital coherent detection, i.e., phase-diversity homodyne detection in combination with DSP, has recently become very attractive in FSO communication systems [36]–[39]. However, as far as we know, almost all the existing mixed RF and coherent FSO systems focus on heterodyne detection [20], [25], and digital coherent detection has never been considered.

In this work, we examine some performance criterions, i.e., the outage probability, the average BER as well as the ergodic capacity (average channel capacity), of a DF-based mixed RF/FSO transmission system with digital coherent detection, whose RF and FSO paths experience the Beaulieu-Xie and the $\mathcal{M}$ fading, respectively. Our main contributions are: (i) We present an end-to-end performance analysis for the DF-based mixed Beaulieu-Xie and $\mathcal{M}$ transmission system. Novel and exact analytical expressions for the cumulative

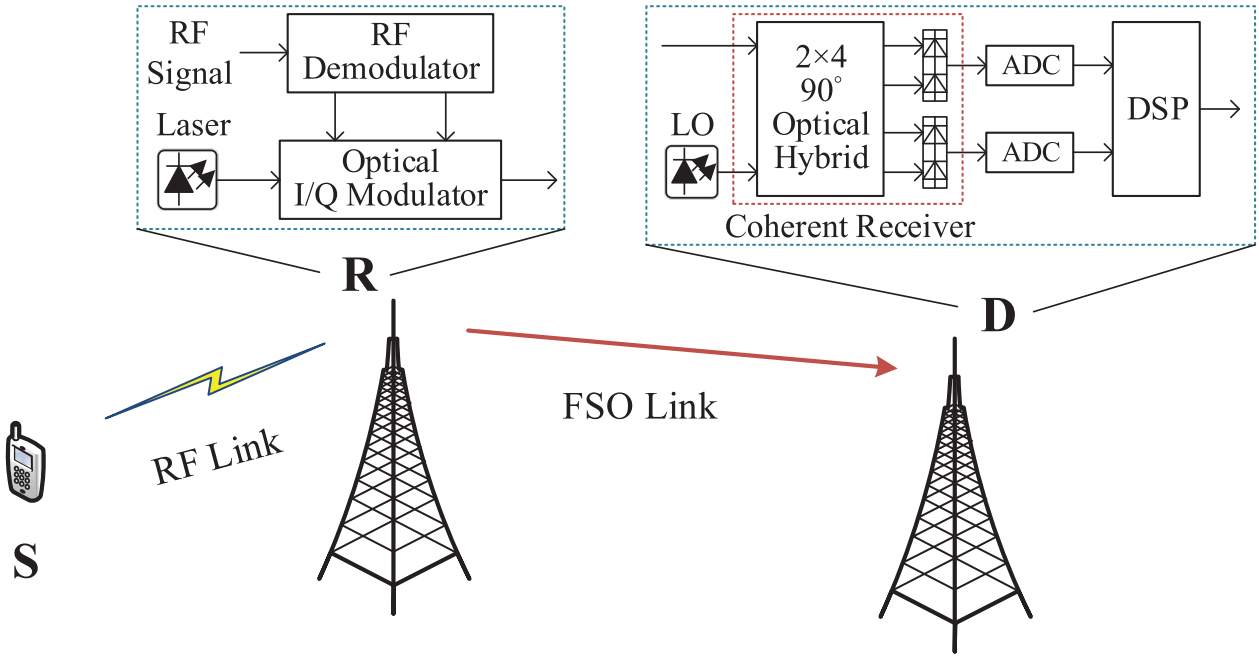

FIGURE 1. System model of the mixed RF/FSO system with digital coherent detection.

distribution function (CDF), the probability density function (PDF) and the moment generating function (MGF) of the overall signal-to-noise ratio (SNR) are derived by means of Meijer's G function [40, eq.(9.301)]. We then derive the outage probability, average BERs of M-ary PSK (MPSK) and M-ary quadrature amplitude modulation (MQAM) with Meijer's G function, and the ergodic capacity with Meijer's G function as well as extended generalized bivariate Meijer's G function (EGBMGF) [41, eq.(1)]. The accurate asymptotic results for the CDF, the MGF, the outage probability, the average BERs, and the ergodic capacity are also given; (ii) As a special case, the exact infinite series expressions are derived for the mixed Beaulieu-Xie and Gamma-Gamma dual-hop transmission system as well; (iii) In order to avoid using the complicated PLL and dealing with high IF, we introduce the digital coherent detection for the FSO hop rather than heterodyne detection.

The rest of the work is organized as follows. We introduce the system and channel models (both RF and FSO) in Section 2. In Section 3, statistical characteristics, such as the CDF, the PDF and the MGF, are derived for the mixed RF/FSO transmission system by means of Meijer's G function. In Section 4, the performance criterions, i.e., the outage probability, the average BERs as well as the ergodic capacity of the system are derived in detail. Section 5 presents some numerical results and discussion. In Section 6, we conclude the work.

II. SYSTEM AND CHANNEL MODELS

A. SYSTEM MODEL

It is assumed that there is no available direct link between the source node (S) and the destination node (D). S needs to communicate with D by means of the intermediate relay node (R), where the DF relaying scheme is employed. The S-R link is an RF link, which subjects to the Beaulieu-Xie fading. The R-D link is an FSO link, and follows $\mathcal{M}$ distribution with zero boresight pointing errors. We employ MPSK and MQAM modulation formats at S. The received RF signal at R is written as

$$y_1 = rs + n_1, \tag{1}$$

where r is the Beaulieu-Xie distributed channel gain of the RF link, s represents the RF signal comes from S, and n_1 indicates the additive white Gaussian noise (AWGN), whose power spectral density (PSD) is N_{01}. The instantaneous SNR per symbol at R is $\gamma_1 = r^2 E_s/N_{01}$. The average SNR per symbol is $\overline{\gamma}_1 = \overline{r^2}E_s/N_{01} = AE_s/N_{01}$, where E_s denotes the energy per symbol, and $A = \overline{r^2}$.

The relay node R decodes the received RF signals and modulates the decoded RF signals over a continuous wave laser beam via an electro-optic Mach-Zehnder in-phase/quadrature (I/Q) modulator. The optical signals from the modulator then propagate along a point-to-point FSO path, which is modeled by $\mathcal{M}$ turbulence with zero boresight pointing errors. At the destination node D, we employ a narrow linewidth local oscillator (LO) and a phase-diversity homodyne receiver [42], which includes a 2×4 90° optical hybrid and two balanced photodiodes, to retrieve the I and Q components of the optical complex amplitude. High-speed ADCs are then used to sample the detected electrical signals, which are processed and recovered by DSP algorithms at last [35]. Figure 1 shows the mixed RF/FSO system, including the schematic diagrams of R and D.

The restored electrical signal at D is written as [35, eq.(24)]

$$i(t) = R\sqrt{P_s P_{\mathrm{LO}}} \exp\{j(\theta_s(t) + \theta_n(t))\} + n_2(t), \quad (2)$$

where P_s denotes the optical power of the instantaneous received signal, and P_{LO} denotes the LO power; R is photodiodes' responsivity; $\theta_s(t)$ and $\theta_n(t)$ are the modulation phase and the total phase noise, respectively; $n_2(t)$ is a zero-mean AWGN process owing to LO induced shot noise [43]. The LO shot noise is expressed as $\overline{i^2_{\mathrm{shot}}} = 2eR\frac{P_{\mathrm{LO}}}{2}\frac{B}{2}$ [42], where $B/2$ denotes the noise bandwidth and e denotes the electron charge. The shot-noise limited SNR per symbol is then derived as [42], [43]

$$\gamma_2 = \frac{|i(t)|^2}{\sigma_n^2} = \frac{|i(t)|^2}{2\overline{i^2_{\mathrm{shot}}}} = \frac{RP_s}{eB} = \frac{\eta P_s}{\hbar f B} = \frac{\eta A_r}{\hbar f B} I, \quad (3)$$

where σ_n^2 is the variance of the total noise, η denotes photodiodes' quantum efficiency, $\hbar$ denotes Planck's constant, f denotes the optical frequency, A_r is the detector area, and I denotes the instant optical irradiance. The average SNR per symbol is defined as $\overline{\gamma}_2 = E[\gamma_2] = \frac{\eta A_r}{\hbar f B} E[I]$, where $E[\cdot]$ denotes the expectation operator.

B. BEAULIEU-XIE FADING MODEL

The Beaulieu-Xie fading model can be derived by introducing a special scale to the non-central chi-distribution distributed variables [29]. The relationship between the Beaulieu-Xie distribution and the Ricean distribution is the same as that between the Nakagami-m model and the Rayleigh distribution; The relationship between the Beaulieu-Xie distribution and the Nakagami-m model is the same as that between the Ricean distribution and the Rayleigh distribution [29]. The PDF of this model is given as [29, eq.(4)]

$$f(r; m, \lambda, \Omega) = \frac{\exp\left[-\frac{m}{\Omega}\left(r^2 + \lambda^2\right)\right] r^m \left(\frac{2m}{\Omega}\right)}{\lambda^{m-1}} \times I_{m-1}\left(\frac{2m}{\Omega}\lambda r\right), \quad (4)$$

where $I_n(\cdot)$ is modified Bessel function of the first kind with nth order; The parameters m and Ω control the shape and the spread of the mode of the Beaulieu-Xie distribution, respectively [29]. The parameter λ exerts an influence on the location and a small impact on the height of the mode [29]. More specifically, m is the fading figure and decides the severity of the fading. λ^2 indicates the power of the LOS components. The K-factor of this model has the same definition as the Ricean model and is expressed as λ^2/Ω. The PDF of the SNR γ_1 is derived by introducing a change of variables in (4) and is expressed as

$$f_{\gamma_1}(\gamma_1) = \frac{m}{\Omega}\left(\frac{A}{\overline{\gamma}_1}\right)^{\frac{m+1}{2}} \frac{J}{\lambda^{m-1}} \gamma_1^{\frac{m-1}{2}} \exp(-\Psi\gamma_1) \times I_{m-1}\left(\frac{2m\lambda}{\Omega}\sqrt{\frac{A\gamma_1}{\overline{\gamma}_1}}\right), \quad (5)$$

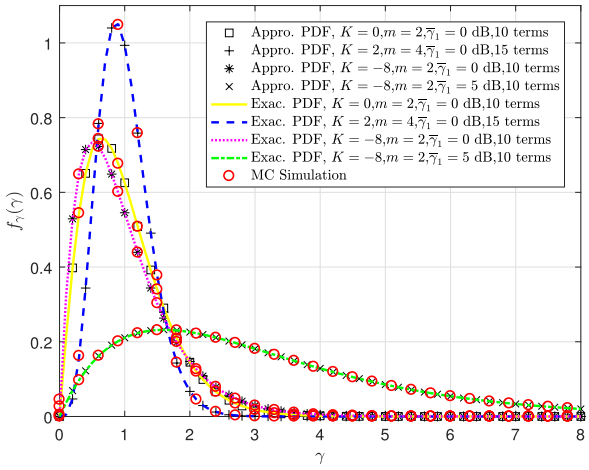

FIGURE 2. The exact expression (5) and the infinite series form (7) with finite summation terms for the PDFs.

where $J = \exp\left(-\frac{m\lambda^2}{\Omega}\right)$ and $\Psi = \frac{mA}{\Omega\overline{\gamma}_1}$. The CDF of γ_1 is derived as

$$F_{\gamma_1}(\gamma_1) = 1 - Q_m\left(\sqrt{\frac{2m}{\Omega}}\lambda, \sqrt{2\Psi\gamma_1}\right), \quad (6)$$

where $Q_v(x, y)$ denotes the generalized Marcum Q-function [44]. By applying the infinite series forms of $I_n(\cdot)$ [45, eq.(9.6.10)] and $Q_v(x, y)$ [44, eq.(4.74)], $f_{\gamma_1}(\gamma_1)$ and $F_{\gamma_1}(\gamma_1)$ can be rewitten as (7) and (8) when m is an integer.

$$f_{\gamma_1}(\gamma_1) = J\exp(-\Psi\gamma_1)\sum_{i=0}^{\infty}\left(\frac{m}{\Omega}\right)^i \frac{\Psi^{i+m}\lambda^{2i}\gamma_1^{i+m-1}}{i!\Gamma(i+m)}, \quad (7)$$

$$F_{\gamma_1}(\gamma_1) = 1 - J\exp(-\Psi\gamma_1)\sum_{i=0}^{\infty}\sum_{j=0}^{i+m-1}\left(\frac{m}{\Omega}\right)^i \frac{\Psi^j\lambda^{2i}\gamma_1^j}{i!j!}, \quad (8)$$

where $\Gamma(\cdot)$ denotes the Gamma function.

The exact expressions ((5) and (6)) and the infinite series representations ((7) and (8)) with finite terms for the PDFs and CDFs of the Beaulieu-Xie model are compared in Figure 2 and Figure 3, respectively. Monte Carlo (MC) simulations are also provided in the figures. Table 1 shows the needed summation terms N_t for the representations (8) under different fading parameters to achieve the required accuracy (e.g., $< 10^{-5}$). The truncation error ϵ_t is defined as $\epsilon_t \triangleq F_{\gamma_1}(\infty) - \hat{F}_{\gamma_1}(\infty)$, where $\hat{F}_{\gamma_1}(\infty)$ denotes the truncated $F_{\gamma_1}(\infty)$ with $i = N_t$ [46]. It can be seen from the table that, if one of the fading parameters (K or m) is fixed, the other parameter increases, or both parameters increase simultaneously, the number of the required summation terms N_t increases. Througth these results, we can draw the conclusion that the infinite series representations for the PDFs and CDFs are convergent with a few summation terms ($N_t \leq 20$) under all considered fading parameters.

C. FSO CHANNEL MODEL

In FSO links, the instantaneous received optical irradiance I is a function of atmospheric turbulence I_a, pointing errors I_p,

TABLE 1. The needed summation terms N_t for the required truncation error ϵ_t under different fading parameters.

Beaulieu-Xie Fading Parameters	N_t	Truncation Error ϵ_t
$K=-8$ dB, $m=2$	5	1.0745×10^{-6}
$K=0$ dB, $m=1$	8	1.1252×10^{-6}
$K=0$ dB, $m=2$	10	8.3082×10^{-6}
$K=0$ dB, $m=3$	13	3.4019×10^{-6}
$K=2$ dB, $m=4$	20	3.3607×10^{-6}

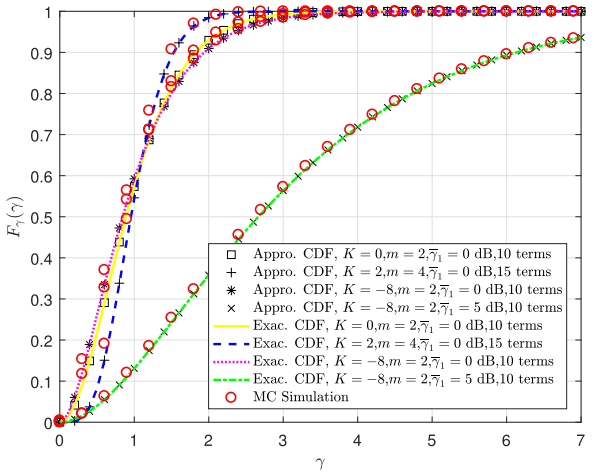

FIGURE 3. The exact expression (6) and the infinite series form (8) with finite summation terms for the CDFs.

and path loss I_l. In this work, we choose the $\mathcal{M}$ statistical model for the atmospheric turbulence, i.e., $I_a \sim \mathcal{M}(\alpha, \beta, g, \rho_m, \Omega')$, where α, β (β is a natural number), g, ρ_m and Ω' indicate the fading parameters associated with the turbulence conditions [32]. It should be noted that the distribution we choose is a particularization of the generalized expression. Owing to its high degree of freedom, the particularization can be utilized to recreate every possible turbulence condition [47]. Since the path loss I_l is deterministic, the PDF of $I = I_l I_a I_p$ can be obtained by using the previous PDFs for I_a [32, eq.(24)] and zero boresight pointing errors I_p [48, eq.(11)] as [49, eq.(5)]

$$f_I(I) = \frac{\xi^2 A_m}{2I}\sum_{k=1}^{\beta} b_k G_{1,3}^{3,0}\left(\frac{\alpha\beta}{g\beta+\Omega'}\frac{I}{A_0 I_l}\middle|\begin{matrix}\xi^2+1\\ \xi^2,\alpha,k\end{matrix}\right), \quad (9)$$

where $\xi = \omega_{z_{\rm eq}}/(2\sigma_s)$, and $\omega_{z_{\rm eq}}$ denotes the equivalent width of the laser beam; $\omega_{z_{\rm eq}}$ is calculated by $\omega_{z_{\rm eq}}^2 = \omega_z^2\sqrt{\pi}\,\mathrm{erf}(\nu)/2\nu\exp(-\nu^2)$, where ω_z denotes the beam waist of the Gaussian laser beam at distance z and $\mathrm{erf}(\cdot)$ denotes the error function; $\nu = \sqrt{\pi}a/\sqrt{2}\omega_z$, where a denotes the detection aperture radius; σ_s is the jitter variance at the destination node D, and A_0 defines the pointing loss. Moreover in (9), α belongs to a positive number and related to large-scale irradiance fluctuations; β indicates the amount of fading; $g = 2b_0(1-\rho_m)$ $(0 \le \rho_m \le 1)$, where $2b_0$ indicates the average power of the whole scatter terms, and ρ_m reveals the amount of optical scattering power coupled into the LOS term; $\Omega' = \Omega_m + \rho_m 2b_0 + 2\sqrt{2b_0\Omega\rho_m}\cos(\phi_A-\phi_B)$, where Ω_m denotes the average power of the LOS component, ϕ_A and ϕ_B are deterministic, representing the phases of the LOS term and the scatter components coupled into the LOS term, respectively; $A_m = \frac{2\alpha^{\frac{\alpha}{2}}}{g^{1+\frac{\alpha}{2}}\Gamma(\alpha)}\left(\frac{g\beta}{g\beta+\Omega'}\right)^{\frac{\alpha}{2}+\beta}$, and $b_k = a_k\left(\alpha\beta/(g\beta+\Omega')\right)^{-\frac{\alpha+k}{2}}$, where $a_k = \binom{\beta-1}{k-1}\frac{1}{(k-1)!}\left(\frac{\Omega'}{g}\right)^{k-1}\left(\frac{\alpha}{\beta}\right)^{\frac{k}{2}}(g\beta+\Omega')^{1-\frac{k}{2}}$ and $\binom{\cdot}{\cdot}$ is the binomial coefficient; $G_{\_,\_}^{\_,\_}(\cdot)$ denotes the Meijer's G function. By using [32, eq.(27)], γ_2 is derived as $\gamma_2 = I\overline{\gamma}_2/E[I] = I\overline{\gamma}_2(\xi^2+1)/\left[I_l\xi^2A_0(g+\Omega')\right]$. Therefore, we can get the PDF of γ_2 with the help of (9) as [49, eq.(6)]

$$f_{\gamma_2}(\gamma_2) = \frac{\xi^2 A_m}{2\gamma_2}\sum_{k=1}^{\beta} b_k G_{1,3}^{3,0}\left(\frac{C\gamma_2}{\overline{\gamma}_2}\middle|\begin{matrix}\kappa_1\\ \kappa_2\end{matrix}\right), \quad (10)$$

where $C = \alpha\beta\xi^2(g+\Omega')/\left[(g\beta+\Omega')(1+\xi^2)\right]$, $\kappa_1 = \xi^2+1$, and $\kappa_2 = \xi^2, \alpha, k$. The CDF of γ_2 is derived as [49, eq.(11)]

$$F_{\gamma_2}(\gamma_2) = \frac{\xi^2 A_m}{2}\sum_{k=1}^{\beta} b_k G_{2,4}^{3,1}\left(\frac{C\gamma_2}{\overline{\gamma}_2}\middle|\begin{matrix}1,\kappa_1\\ \kappa_2,0\end{matrix}\right). \quad (11)$$

We can get the PDF for the Gamma-Gamma model by setting $\rho_m = 1$ and $\Omega' = 1$ in (10) as [49, eq.(10)]

$$f_{\gamma_2}(\gamma_2) = \frac{B_g}{\gamma_2}G_{1,3}^{3,0}\left(\frac{D\gamma_2}{\overline{\gamma}_2}\middle|\begin{matrix}\kappa_1\\ \kappa_3\end{matrix}\right), \quad (12)$$

where $B_g = \xi^2/(\Gamma(\alpha)\Gamma(\beta))$, $D = \alpha\beta\xi^2/(\xi^2+1)$ and $\kappa_3 = \xi^2, \alpha, \beta$. The CDF for the Gamma-Gamma model is [49, eq.(12)]

$$F_{\gamma_2}(\gamma_2) = B_g G_{2,4}^{3,1}\left(\frac{D\gamma_2}{\overline{\gamma}_2}\middle|\begin{matrix}1,\kappa_1\\ \kappa_3,0\end{matrix}\right). \quad (13)$$

III. STATISTICAL CHARACTERISTICS

A. CUMULATIVE DISTRIBUTION FUNCTION

As for DF transmission, the relay need to fully decode the source message. The overall SNR for a DF-based mixed RF/FSO transmission system can be written as [50]

$$\gamma = \min(\gamma_1, \gamma_2). \quad (14)$$

Therefore, the CDF of γ is expressed as [50]

$$\begin{aligned} F_\gamma(\gamma) &= \Pr(\min(\gamma_1,\gamma_2) < \gamma) \\ &= F_{\gamma_1}(\gamma) + F_{\gamma_2}(\gamma) - F_{\gamma_1}(\gamma)F_{\gamma_2}(\gamma) \\ &= 1 + Q_m\left(\sqrt{\frac{2m}{\Omega}}\lambda, \sqrt{2\Psi\gamma}\right) \\ &\quad\times\left[\frac{\xi^2 A_m}{2}\sum_{k=1}^{\beta} b_k G_{2,4}^{3,1}\left(\frac{C\gamma}{\overline{\gamma}_2}\middle|\begin{matrix}1,\kappa_1\\ \kappa_2,0\end{matrix}\right) - 1\right]. \end{aligned} \quad (15)$$

When the FSO link follows Gamma-Gamma distribution, we can get the CDF as

$$F_\gamma(\gamma) = 1 + Q_m\left(\sqrt{\frac{2m}{\Omega}}\lambda, \sqrt{2\Psi\gamma}\right) \times \left[B_g G_{2,4}^{3,1}\left(\frac{D\gamma}{\overline{\gamma}_2}\middle| \begin{matrix}1, \kappa_1\\ \kappa_3, 0\end{matrix}\right) - 1\right]. \quad (16)$$

Asymptotic Analysis: When $\overline{\gamma}_2 \to \infty$, $\frac{C\gamma}{\overline{\gamma}_2} \to 0$, with the aid of [51, eq.(07.34.06.0006.01)], we can get the asymptotoc expression for the CDF in (15) as

$$F_\gamma(\gamma) \approx 1 + Q_m\left(\sqrt{\frac{2m}{\Omega}}\lambda, \sqrt{2\Psi\gamma}\right) \times \left[\frac{\xi^2 A_m}{2}\sum_{k=1}^{\beta} b_k \sum_{\varepsilon=1}^{3}\left(\frac{C\gamma}{\overline{\gamma}_2}\right)^{\kappa_{2,\varepsilon}} \times \frac{\prod_{\tau=1,\tau\neq\varepsilon}^{3}\Gamma\left(\kappa_{2,\tau}-\kappa_{2,\varepsilon}\right)}{\kappa_{2,\varepsilon}\Gamma\left(\xi^2+1-\kappa_{2,\varepsilon}\right)} - 1\right]. \quad (17)$$

When $\overline{\gamma}_2 \to \infty$, $\frac{D\gamma}{\overline{\gamma}_2} \to 0$, we can also get the asymptotoc expression of CDF for the mixed Beaulieu-Xie and Gamma-Gamma system as

$$F_\gamma(\gamma) \approx 1 + Q_m\left(\sqrt{\frac{2m}{\Omega}}\lambda, \sqrt{2\Psi\gamma}\right) \times \left[B_g \sum_{\varepsilon=1}^{3}\left(\frac{D\gamma}{\overline{\gamma}_2}\right)^{\kappa_{3,\varepsilon}} \frac{\prod_{\tau=1,\tau\neq\varepsilon}^{3}\Gamma\left(\kappa_{3,\tau}-\kappa_{3,\varepsilon}\right)}{\kappa_{3,\varepsilon}\Gamma\left(\xi^2+1-\kappa_{3,\varepsilon}\right)} - 1\right]. \quad (18)$$

B. PROBABILITY DENSITY FUNCTION

We can get the PDF by taking the derivative of (15) in respect to γ as (19), as shown at the top of the next page. When the FSO link is Gamma-Gamma model, the PDF is expressed as (20), as shown at the top of the next page.

C. MOMENT GENERATING FUNCTION

The MGF of γ is defined by $M_\gamma(s) = E\left[e^{-\gamma s}\right]$ [20]. With the help of integration by parts and (15), we can get the MGF of γ as

$$M_\gamma(s) = s\int_0^\infty e^{-\gamma s} F_\gamma(\gamma)\, d\gamma = 1 + sJ\sum_{i=0}^{\infty}\sum_{j=0}^{i+m-1}\left(\frac{m}{\Omega}\right)^i \frac{\Psi^j\lambda^{2i}}{i!J_s^{j+1}} \times \left[\frac{\xi^2 A_m}{2}\sum_{k=1}^{\beta}\frac{b_k}{j!}G_{3,4}^{3,2}\left(\frac{C}{\overline{\gamma}_2 J_s}\middle| \begin{matrix}-j, 1, \kappa_1\\ \kappa_2, 0\end{matrix}\right) - 1\right], \quad (21)$$

where $J_s = \Psi + s$. When the FSO path experiences Gamma-Gamma fading, the MGF is derived as

$$M_\gamma(s) = 1 + sJ\sum_{i=0}^{\infty}\sum_{j=0}^{i+m-1}\left(\frac{m}{\Omega}\right)^i \frac{\Psi^j\lambda^{2i}}{i!J_s^{j+1}} \times \left[\frac{B_g}{j!}G_{3,4}^{3,2}\left(\frac{D}{\overline{\gamma}_2 J_s}\middle| \begin{matrix}-j, 1, \kappa_1\\ \kappa_3, 0\end{matrix}\right) - 1\right]. \quad (22)$$

Asymptotic Analysis: When $\overline{\gamma}_2 \to \infty$, $\frac{C}{\overline{\gamma}_2 J_s} \to 0$, with the help of the asymptotic series of Meijer's G function [51, eq.(07.34.06.0006.01)], the asymptotoc expression for (21) is expressed as

$$M_\gamma(s) \approx 1 + sJ\sum_{i=0}^{\infty}\sum_{j=0}^{i+m-1}\left(\frac{m}{\Omega}\right)^i \frac{\Psi^j\lambda^{2i}}{i!J_s^{j+1}} \times \left[\frac{\xi^2 A_m}{2}\sum_{k=1}^{\beta}\frac{b_k}{j!}\sum_{\varepsilon=1}^{3}\left(\frac{C}{\overline{\gamma}_2 J_s}\right)^{\kappa_{2,\varepsilon}} \times \frac{\prod_{\tau=1,\tau\neq\varepsilon}^{3}\Gamma\left(\kappa_{2,\tau}-\kappa_{2,\varepsilon}\right)\Gamma\left(j+1+\kappa_{2,\varepsilon}\right)}{\kappa_{2,\varepsilon}\Gamma\left(\xi^2+1-\kappa_{2,\varepsilon}\right)} - 1\right]. \quad (23)$$

When $\overline{\gamma}_2 \to \infty$, $\frac{D}{\overline{\gamma}_2 J_s} \to 0$, the asymptotoc expression for (22) is expressed as (24), as shown at the top of the next page.

IV. PERFORMANCE ANALYSIS

A. OUTAGE PROBABILITY

As an important performance criterion for digital communication systems subjecting to fading channels [44], outage probability is defined by the probability that the equivalent SNR γ falls below a given threshold γ_{th} [44], and it is obtained by setting $\gamma = \gamma_{\text{th}}$ in (15) and (16) as

$$P_{\text{out}}(\gamma_{\text{th}}) = F_\gamma(\gamma_{\text{th}}). \quad (25)$$

Asymptotic Analysis: We can get the asymptotic expressions for (25) by replacing γ in (17) and (18) with γ_{th}, respectively. The diversity order of the mixed RF/FSO transmission system is $G_d = \min\left\{m, \min\left\{\xi^2, \alpha, k\right\}\right\}$. When the FSO path follows Gamma-Gamma distribution, the diversity order is $G_d = \min\left\{m, \min\left\{\xi^2, \alpha, \beta\right\}\right\}$. The detailed derivation is presented in Appendix A.

B. AVERAGE BER

Besides improving the receiver sensitivity, higher-order modulation formats, such as MPSK and MQAM, are often used to further increase spectral efficiency for the coherent optical communication systems. As for the coherent MPSK scheme,

$$f_\gamma(\gamma) = f_{\gamma_1}(\gamma) + f_{\gamma_2}(\gamma) - f_{\gamma_1}(\gamma) F_{\gamma_2}(\gamma) - F_{\gamma_1}(\gamma) f_{\gamma_2}(\gamma)$$
$$= \frac{m}{\Omega}\left(\frac{A}{\overline{\gamma}_1}\right)^{\frac{m+1}{2}} \frac{J}{\lambda^{m-1}} \gamma^{\frac{m-1}{2}} \exp(-\Psi\gamma) I_{m-1}\left(\frac{2m\lambda}{\Omega}\sqrt{\frac{A\gamma}{\overline{\gamma}_1}}\right)\left[1 - \frac{\xi^2 A_m}{2}\sum_{k=1}^{\beta} b_k G_{2,4}^{3,1}\left(\frac{C\gamma}{\overline{\gamma}_2}\middle|\begin{matrix}1, \kappa_1\\ \kappa_2, 0\end{matrix}\right)\right]$$
$$+ \frac{\xi^2 A_m}{2\gamma}\sum_{k=1}^{\beta} b_k G_{1,3}^{3,0}\left(\frac{C\gamma}{\overline{\gamma}_2}\middle|\begin{matrix}\kappa_1\\ \kappa_2\end{matrix}\right) Q_m\left(\sqrt{\frac{2m}{\Omega}}\lambda, \sqrt{2\Psi\gamma}\right). \quad (19)$$

$$f_\gamma(\gamma) = \frac{m}{\Omega}\left(\frac{A}{\overline{\gamma}_1}\right)^{\frac{m+1}{2}} \frac{J}{\lambda^{m-1}} \gamma^{\frac{m-1}{2}} \exp(-\Psi\gamma) I_{m-1}\left(\frac{2m\lambda}{\Omega}\sqrt{\frac{A\gamma}{\overline{\gamma}_1}}\right)\left[1 - B_g G_{2,4}^{3,1}\left(\frac{D\gamma}{\overline{\gamma}_2}\middle|\begin{matrix}1, \kappa_1\\ \kappa_3, 0\end{matrix}\right)\right]$$
$$+ \frac{B_g}{\gamma} G_{1,3}^{3,0}\left(\frac{D\gamma}{\overline{\gamma}_2}\middle|\begin{matrix}\kappa_1\\ \kappa_3\end{matrix}\right) Q_m\left(\sqrt{\frac{2m}{\Omega}}\lambda, \sqrt{2\Psi\gamma}\right). \quad (20)$$

$$M_\gamma(s) \approx 1 + sJ\sum_{i=0}^{\infty}\sum_{j=0}^{i+m-1}\left(\frac{m}{\Omega}\right)^i \frac{\Psi^j \lambda^{2i}}{i! J_s^{j+1}}\left[\frac{B_g}{j!}\sum_{\varepsilon=1}^{3}\left(\frac{D}{\overline{\gamma}_2 J_s}\right)^{\kappa_{3,\varepsilon}} \frac{\prod_{\tau=1,\tau\neq\varepsilon}^{3}\Gamma(\kappa_{3,\tau} - \kappa_{3,\varepsilon})\Gamma(j+1+\kappa_{3,\varepsilon})}{\kappa_{3,\varepsilon}\Gamma(\xi^2+1-\kappa_{3,\varepsilon})} - 1\right]. \quad (24)$$

$$P_b(e) = \sum_{p=1}^{\max(M/4,1)} K_1 + \frac{JK_1}{\sqrt{\pi}}\sum_{p=1}^{\max(M/4,1)}\sum_{i=0}^{\infty}\sum_{j=0}^{i+m-1}\left(\frac{m}{\Omega}\right)^i \frac{u_p \Psi^j \lambda^{2i}}{i! j! U_p^{j+\frac{1}{2}}}$$
$$\times\left[\frac{\xi^2 A_m}{2}\sum_{k=1}^{\beta} b_k G_{3,4}^{3,2}\left(\frac{C}{\overline{\gamma}_2 U_p}\middle|\begin{matrix}\frac{1}{2}-j, 1, \kappa_1\\ \kappa_2, 0\end{matrix}\right) - \Gamma\left(j+\frac{1}{2}\right)\right], \quad (28)$$

the conditional BER is expressed as [22, eq.(27)]

$$P_{b,M\text{PSK}}(e|\gamma) \cong \frac{2}{\max(\log_2 M, 2)}\sum_{p=1}^{\max(M/4,1)} Q\left(u_p\sqrt{2\gamma}\right), \quad (26)$$

where $u_p = \sin\frac{(2p-1)\pi}{M}$, and $Q(x)$ denotes the Q-function. The average BER is expressed as [22, eq.(28)]

$$P_b(e) = \int_0^\infty P_{b,M\text{PSK}}(e|\gamma) f_\gamma(\gamma)\, d\gamma$$
$$= -\int_0^\infty F_\gamma(\gamma)\, dP_{b,M\text{PSK}}(e|\gamma). \quad (27)$$

With the aid of [51, eq.(07.34.21.0088.01)] and [40, eq.(3.381.4)], the average BER is derived as (28), as shown at the top of this page, where $K_1 = 1/\max(\log_2 M, 2)$ and $U_p = \Psi + u_p^2$. When the FSO link subjects to the Gamma-Gamma fading, the average BER can be derived as

$$P_b(e) = \sum_{p=1}^{\max(M/4,1)} K_1 + \frac{JK_1}{\sqrt{\pi}}\sum_{p=1}^{\max(M/4,1)}\sum_{i=0}^{\infty}\sum_{j=0}^{i+m-1}\left(\frac{m}{\Omega}\right)^i$$
$$\times\frac{u_p \Psi^j \lambda^{2i}}{i! j! U_p^{j+\frac{1}{2}}}\left[B_g G_{3,4}^{3,2}\left(\frac{D}{\overline{\gamma}_2 U_p}\middle|\begin{matrix}\frac{1}{2}-j, 1, \kappa_1\\ \kappa_3, 0\end{matrix}\right) - \Gamma\left(j+\frac{1}{2}\right)\right]. \quad (29)$$

As for MQAM, the conditional BER is expressed as [22, eq.(32)]

$$P_{b,M\text{QAM}}(e|\gamma) \cong 4K_2\sum_{p=1}^{\sqrt{M}/2} Q\left(v_p\sqrt{\gamma}\right), \quad (30)$$

where $K_2 = \frac{1}{\log_2 M}\left(1 - \frac{1}{\sqrt{M}}\right)$, and $v_p = (2p-1)\sqrt{\frac{3}{M-1}}$. The average BER is derived as

$$P_b(e) = \sum_{p=1}^{\sqrt{M}/2} 2K_2 + \frac{JK_2}{\sqrt{2\pi}}\sum_{p=1}^{\sqrt{M}/2}\sum_{i=0}^{\infty}\sum_{j=0}^{i+m-1}\left(\frac{m}{\Omega}\right)^i \frac{v_p \Psi^j \lambda^{2i}}{i! j! V_p^{j+\frac{1}{2}}}$$
$$\times\left[\xi^2 A_m\sum_{k=1}^{\beta} b_k G_{3,4}^{3,2}\left(\frac{C}{\overline{\gamma}_2 V_p}\middle|\begin{matrix}\frac{1}{2}-j, 1, \kappa_1\\ \kappa_2, 0\end{matrix}\right) - 2\Gamma\left(j+\frac{1}{2}\right)\right], \quad (31)$$

where $V_p = \Psi + \frac{v_p^2}{2}$. The average BER for the cooperative system in the presence of Gamma-Gamma fading can be expressed as

$$P_b(e) = \sum_{p=1}^{\sqrt{M}/2} 2K_2 + \frac{\sqrt{2}JK_2}{\sqrt{\pi}}\sum_{p=1}^{\sqrt{M}/2}\sum_{i=0}^{\infty}\sum_{j=0}^{i+m-1}\left(\frac{m}{\Omega}\right)^i$$
$$\times\frac{v_p \Psi^j \lambda^{2i}}{i! j! V_p^{j+\frac{1}{2}}}\left[B_g G_{3,4}^{3,2}\left(\frac{D}{\overline{\gamma}_2 V_p}\middle|\begin{matrix}\frac{1}{2}-j, 1, \kappa_1\\ \kappa_3, 0\end{matrix}\right) - \Gamma\left(j+\frac{1}{2}\right)\right]. \quad (32)$$

Asymptotic Analysis: As for MPSK, when $\overline{\gamma}_2 \to \infty$, $\frac{C}{\overline{\gamma}_2 U_p} \to 0$, the asymptotoc expression for (28) is expressed as (33), as shown at the bottom of the next page. When $\overline{\gamma}_2 \to \infty$, $\frac{D}{\overline{\gamma}_2 U_p} \to 0$, the asymptotoc expression for (29) is expressed as (34), as shown at the bottom of the next page.

As for MQAM, when $\overline{\gamma}_2 \to \infty$, $\frac{C}{\overline{\gamma}_2 V_p} \to 0$, the asymptotoc expression for (31) is expressed as (35), as shown at the bottom of the next page. When $\overline{\gamma}_2 \to \infty$, $\frac{D}{\overline{\gamma}_2 V_p} \to 0$, the asymptotoc expression for (32) is expressed as (36), as shown at the bottom of the next page.

C. ERGODIC CAPACITY

Since the atmospheric turbulence is varying on the order of several milliseconds, the FSO fading has minor change over the duration of millions of consecutive bits [49]. The ergodic channel capacity represents the best achievable capacity for the FSO link [49], and it can be written by means of the complementary CDF (CCDF) as [20, eq.(26)]

$$C_{\text{ec}} = \frac{1}{\ln(2)} \int_0^\infty \frac{F_\gamma^c(\gamma)}{1+\gamma} d\gamma, \tag{37}$$

where $F_\gamma^c(\gamma) = 1 - F_\gamma(\gamma)$. With the aid of the Meijer's G function representations for $(1+x)^\alpha$ [52, eq.(10)] and e^{-x} [52, eq.(11)], we can calculate the integral (37) as (38), as shown at the bottom of the next page, where $G_{-,-:-,-:-,-}^{-,-:-,-:-,-}(\cdot)$ is EGBMGF. When the dual-hop system operates over Gamma-Gamma fading, the ergodic capacity is derived as

$$C_{\text{ec}} = \frac{J}{\ln(2)} \sum_{i=0}^{\infty} \sum_{j=0}^{i+m-1} \left(\frac{m}{\Omega}\right)^i \frac{\lambda^{2i}}{i!j!\Psi} \left[G_{2,1}^{1,2}\left(\frac{1}{\Psi} \middle| \begin{matrix} -j, 0 \\ 0 \end{matrix} \right) - B_g G_{1,0:2,4:1,1}^{1,0:3,1:1,1}\left(\begin{matrix} j+1 \\ - \end{matrix} \middle| \begin{matrix} 1, \kappa_1 \\ \kappa_3, 0 \end{matrix} \middle| \begin{matrix} 0 \\ 0 \end{matrix} \middle| \frac{D}{\Psi\overline{\gamma}_2}, \frac{1}{\Psi} \right) \right]. \tag{39}$$

Asymptotic Analysis: In the case of $\overline{\gamma}_1 \neq \overline{\gamma}_2$, when $\overline{\gamma}_2 \to \infty$, we get $\frac{C}{\Psi\overline{\gamma}_2} \to 0$, and the asymptotic expression for (38) is derived as (40), as shown at the bottom of the 10th page, where $\kappa_{2,\vartheta} = \min\{\xi^2, \alpha, k\}$. When $\frac{D}{\Psi\overline{\gamma}_2} \to 0$, the asymptotic expression for (39) is derived as (41), as shown at the bottom of the 10th page, where $\kappa_{3,\vartheta} = \min\{\xi^2, \alpha, \beta\}$.

As for $\overline{\gamma}_1 = \overline{\gamma}_2$, when $\overline{\gamma}_2 \to \infty$, we get $\frac{C}{\Psi\overline{\gamma}_2} = \frac{C\Omega}{mA}$, which is a constant, and $\frac{1}{\Psi} \to \infty$. The asymptotic expression for (38) is derived as

$$C_{\text{ec}} \approx \frac{J}{\ln(2)} \sum_{i=0}^{\infty} \sum_{j=0}^{i+m-1} \left(\frac{m}{\Omega}\right)^i \frac{\lambda^{2i}}{i!j!} \left[\Gamma(j) - \frac{\xi^2 A_m}{2} \sum_{k=1}^{\beta} b_k G_{3,4}^{3,2}\left(\frac{C}{\Psi\overline{\gamma}_2} \middle| \begin{matrix} 1-j, 1, \kappa_1 \\ \kappa_2, 0 \end{matrix} \right) \right]. \tag{42}$$

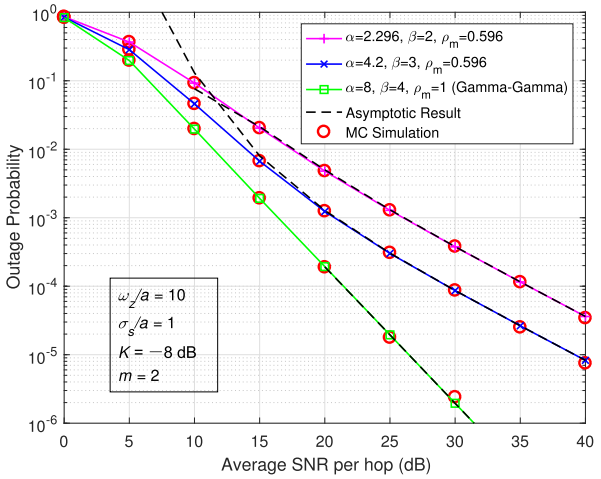

FIGURE 4. Outage probability versus average SNR per hop under weak, moderate and strong turbulence conditions with fixed pointing error effect $\sigma_s/a = 1$.

When $\frac{D}{\Psi\overline{\gamma}_2}$ is a constant and $\frac{1}{\Psi} \to \infty$, the asymptotic expression for (39) is derived as

$$C_{\text{ec}} \approx \frac{J}{\ln(2)} \sum_{i=0}^{\infty} \sum_{j=0}^{i+m-1} \left(\frac{m}{\Omega}\right)^i \frac{\lambda^{2i}}{i!j!} \left[\Gamma(j) - B_g G_{3,4}^{3,2}\left(\frac{D}{\Psi\overline{\gamma}_2} \middle| \begin{matrix} 1-j, 1, \kappa_1 \\ \kappa_3, 0 \end{matrix} \right) \right]. \tag{43}$$

The detailed derivation is given in Appendix B.

V. NUMERICAL RESULTS AND DISCUSSION

In this part, numerical results for the derived expressions above of the outage probability, average BERs and the ergodic capacity are presented. MC simulations are also carried out to confirm the analytical results. For the RF link, the parameters $K = -8$ dB, $m = 2, 3$ are used as in [29]. For the FSO path, the weak, moderate, and strong turbulence scenarios are reproduced by employing (8, 4), (4.2, 3), and (2.296, 2) for the parameters (α, β) as in [26], [49]. The impact of the pointing error is described by the normalized beamwidth ω_z/a and the normalized jitter σ_s/a. When ω_z/a is fixed, the lower value of σ_s/a, the weaker effect of the pointing error. Other parameters are as follows: $\Omega_m = 1.3265$, $b_0 = 0.1079$, $\rho_m = 0.596$, and $\phi_A - \phi_B = \pi/2$; The FSO link distance L is 1 km, the optical wavelength λ is 785 nm, and the detection aperture radius a is 5 cm. Note that Meijer's G function is a built-in function of some computing software, e.g., MATLAB and MATHEMATICA, and the detailed MATLAB and MATHEMATICA code for the EGBMGF can be found in [53] and [54], respectively.

Figure 4 and 5 show the outage probability of the proposed dual-hop system versus the average SNR per link ($\overline{\gamma}_1 = \overline{\gamma}_2$) under weak, moderate and strong turbulence scenarios with varying pointing error effects ($\sigma_s/a = 1$ and $\sigma_s/a = 5$). γ_{th} is fixed at 0 dB. According to the figures, it is noticeable that the analytical results (25) matches very well with the

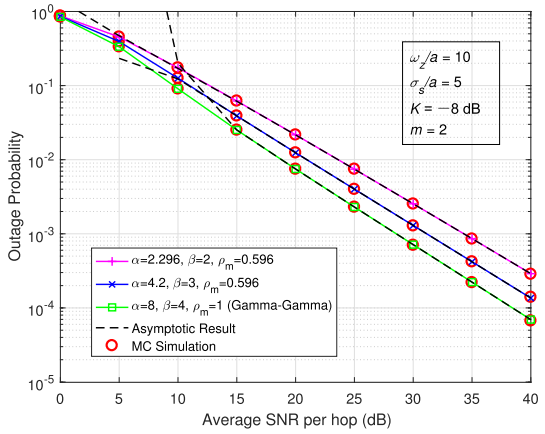

FIGURE 5. Outage probability versus average SNR per hop under weak, moderate and strong turbulence conditions with fixed pointing error effect $\sigma_s/a = 5$.

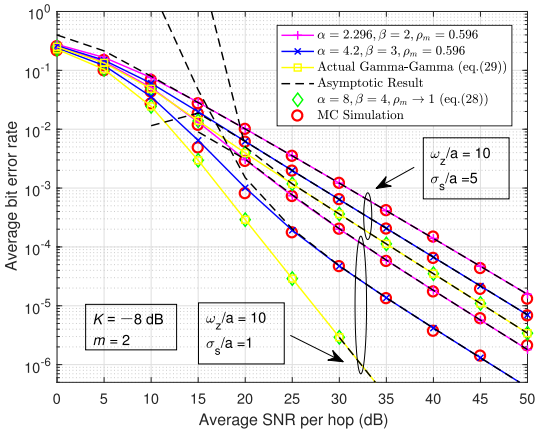

FIGURE 6. Average BER versus average SNR per hop for QPSK under weak, moderate and strong turbulence conditions with varying pointing error effects.

MC simulation results. The simulation results of the $\mathcal{M}$ turbulence (by setting $\rho_m \to 1$) are in good agreement with the numerical results of Gamma-Gamma fading (16). As expected, the severer the effect of turbulence conditions and zero boresight pointing errors, the poorer the outage performance of the dual-hop system. In addition, the asymptotic

$$P_b(e) \approx \sum_{p=1}^{\max(M/4,1)} K_1 + \frac{JK_1}{\sqrt{\pi}} \sum_{p=1}^{\max(M/4,1)} \sum_{i=0}^{\infty} \sum_{j=0}^{i+m-1} \left(\frac{m}{\Omega}\right)^i \frac{u_p \Psi^j \lambda^{2i}}{i!j! U_p^{j+\frac{1}{2}}} \left[\frac{\xi^2 A_m}{2} \sum_{k=1}^{\beta} b_k \sum_{\varepsilon=1}^{3} \left(\frac{C}{\overline{\gamma}_2 U_p}\right)^{\kappa_{2,\varepsilon}} \times \frac{\prod_{\tau=1,\tau\neq\varepsilon}^{3} \Gamma\left(\kappa_{2,\tau} - \kappa_{2,\varepsilon}\right) \Gamma\left(j + \frac{1}{2} + \kappa_{2,\varepsilon}\right)}{\kappa_{2,\varepsilon} \Gamma\left(\xi^2 + 1 - \kappa_{2,\varepsilon}\right)} - \Gamma\left(j + \frac{1}{2}\right) \right]. \tag{33}$$

$$P_b(e) \approx \sum_{p=1}^{\max(M/4,1)} K_1 + \frac{JK_1}{\sqrt{\pi}} \sum_{p=1}^{\max(M/4,1)} \sum_{i=0}^{\infty} \sum_{j=0}^{i+m-1} \left(\frac{m}{\Omega}\right)^i \frac{u_p \Psi^j \lambda^{2i}}{i!j! U_p^{j+\frac{1}{2}}} \left[B_g \sum_{\varepsilon=1}^{3} \left(\frac{D}{\overline{\gamma}_2 U_p}\right)^{\kappa_{3,\varepsilon}} \times \frac{\prod_{\tau=1,\tau\neq\varepsilon}^{3} \Gamma\left(\kappa_{3,\tau} - \kappa_{3,\varepsilon}\right) \Gamma\left(j + \frac{1}{2} + \kappa_{3,\varepsilon}\right)}{\kappa_{3,\varepsilon} \Gamma\left(\xi^2 + 1 - \kappa_{3,\varepsilon}\right)} - \Gamma\left(j + \frac{1}{2}\right) \right]. \tag{34}$$

$$P_b(e) \approx \sum_{p=1}^{\sqrt{M}/2} 2K_2 + \frac{JK_2}{\sqrt{2\pi}} \sum_{p=1}^{\sqrt{M}/2} \sum_{i=0}^{\infty} \sum_{j=0}^{i+m-1} \left(\frac{m}{\Omega}\right)^i \frac{v_p \Psi^j \lambda^{2i}}{i!j! V_p^{j+\frac{1}{2}}} \left[\xi^2 A_m \sum_{k=1}^{\beta} b_k \sum_{\varepsilon=1}^{3} \left(\frac{C}{\overline{\gamma}_2 V_p}\right)^{\kappa_{2,\varepsilon}} \times \frac{\prod_{\tau=1,\tau\neq\varepsilon}^{3} \Gamma\left(\kappa_{2,\tau} - \kappa_{2,\varepsilon}\right) \Gamma\left(j + \frac{1}{2} + \kappa_{2,\varepsilon}\right)}{\kappa_{2,\varepsilon} \Gamma\left(\xi^2 + 1 - \kappa_{2,\varepsilon}\right)} - 2\Gamma\left(j + \frac{1}{2}\right) \right]. \tag{35}$$

$$P_b(e) \approx \sum_{p=1}^{\sqrt{M}/2} 2K_2 + \frac{\sqrt{2}JK_2}{\sqrt{\pi}} \sum_{p=1}^{\sqrt{M}/2} \sum_{i=0}^{\infty} \sum_{j=0}^{i+m-1} \left(\frac{m}{\Omega}\right)^i \frac{v_p \Psi^j \lambda^{2i}}{i!j! V_p^{j+\frac{1}{2}}} \left[B_g \sum_{\varepsilon=1}^{3} \left(\frac{D}{\overline{\gamma}_2 V_p}\right)^{\kappa_{3,\varepsilon}} \times \frac{\prod_{\tau=1,\tau\neq\varepsilon}^{3} \Gamma\left(\kappa_{3,\tau} - \kappa_{3,\varepsilon}\right) \Gamma\left(j + \frac{1}{2} + \kappa_{3,\varepsilon}\right)}{\kappa_{3,\varepsilon} \Gamma\left(\xi^2 + 1 - \kappa_{3,\varepsilon}\right)} - \Gamma\left(j + \frac{1}{2}\right) \right]. \tag{36}$$

$$C_{\text{ec}} = \frac{J}{\ln(2)} \sum_{i=0}^{\infty} \sum_{j=0}^{i+m-1} \left(\frac{m}{\Omega}\right)^i \frac{\lambda^{2i}}{i!j!\Psi} \left[G_{2,1}^{1,2}\left(\frac{1}{\Psi} \middle| \begin{matrix} -j, 0 \\ 0 \end{matrix}\right) - \frac{\xi^2 A_m}{2} \sum_{k=1}^{\beta} b_k G_{1,0:2,4:1,1}^{1,0:3,1:1,1}\left(\begin{matrix} j+1 \\ - \end{matrix} \middle| \begin{matrix} 1, \kappa_1 \\ \kappa_2, 0 \end{matrix} \middle| \begin{matrix} 0 \\ 0 \end{matrix} \middle| \frac{C}{\Psi \overline{\gamma}_2}, \frac{1}{\Psi} \right) \right], \tag{38}$$

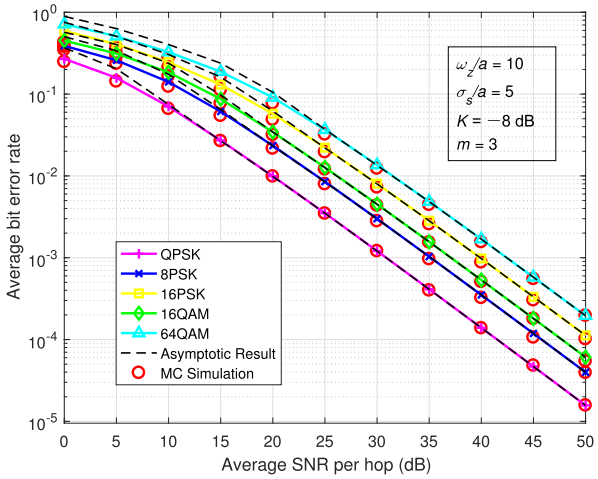

FIGURE 7. Average BER versus average SNR per hop for different modulation formats under the strong turbulence condition with fixed pointing error effect $\sigma_s/a = 5$.

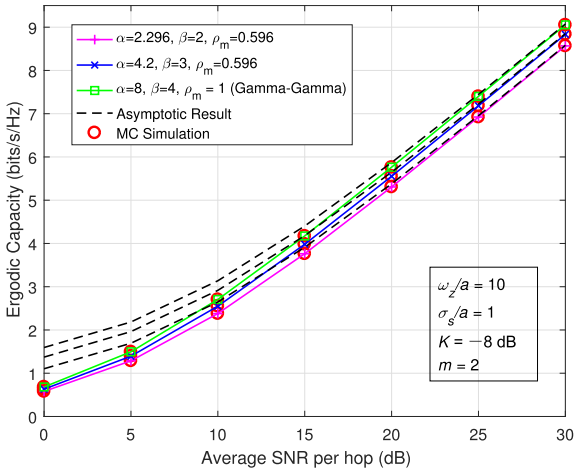

FIGURE 8. Ergodic capacity versus average SNR per hop under weak, moderate and strong turbulence conditions with fixed pointing error effect $\sigma_s/a = 1$.

results ((17) and (18)) are also given in the figures. We can find that the asymptotic results converge fast to the exact results when the SNR is high.

The average BERs versus the average SNR per link are presented in Figure 6 and 7. It can be found from the figures that the analytical results are consistent with the MC simulation results as well. Figure 6 plots the average BERs of QPSK experiencing weak, moderate and strong turbulence conditions with varying pointing error effects ($\sigma_s/a = 1$ and $\sigma_s/a = 5$). As shown in the figure, when the $\mathcal{M}$ turbulence gets strong and the value of the normalized jitter σ_s/a increases (the normalized beamwidth ω_z/a is fixed at 10), the BER performance deteriorates. Expectedly, the analytical results of the $\mathcal{M}$ distribution (28) are accordant with those for the Gamma-Gamma distribution (29). The average BERs of QPSK, 8PSK, 16PSK, 16QAM and 64QAM subjecting to the strong turbulence with fixed pointing error effect $\sigma_s/a = 5$ are displayed in Figure 7. By comparing the BER curves for QPSK propagating through the strong turbulence with fixed pointing error effect $\sigma_s/a = 5$ in Figure 6 and 7, we can get the similar conclusion to [50] that the FSO path acts the dominant role between the two hops, since the stronger effect of RF fading ($m = 2$) has little influence on the average BER performance. Furthermore, the asymptotic results in these figures are in an excellent agreement with the exact results in the high SNR regime.

$$C_{\rm ec} \approx \frac{J}{\ln(2)} \sum_{i=0}^{\infty} \sum_{j=0}^{i+m-1} \left(\frac{m}{\Omega}\right)^i \frac{\lambda^{2i}}{i!j!\Psi} \left[G_{2,1}^{1,2}\left(\frac{1}{\Psi}\middle|\begin{matrix}-j,0\\0\end{matrix}\right) - \frac{\xi^2 A_m}{2} \frac{\Gamma(\kappa_{2,\vartheta}) \prod_{\tau=1,\tau\neq\vartheta}^{3} \Gamma(\kappa_{2,\tau}-\kappa_{2,\vartheta})}{\Gamma(\xi^2+1-\kappa_{2,\vartheta})\Gamma(1+\kappa_{2,\vartheta})} \left(\frac{C}{\Psi\overline{\gamma}_2}\right)^{\kappa_{2,\vartheta}} \sum_{k=1}^{\beta} b_k G_{2,1}^{1,2}\left(\frac{1}{\Psi}\middle|\begin{matrix}-j-\kappa_{2,\vartheta},0\\0\end{matrix}\right) \right], \tag{40}$$

$$C_{\rm ec} \approx \frac{J}{\ln(2)} \sum_{i=0}^{\infty} \sum_{j=0}^{i+m-1} \left(\frac{m}{\Omega}\right)^i \frac{\lambda^{2i}}{i!j!\Psi} \left[G_{2,1}^{1,2}\left(\frac{1}{\Psi}\middle|\begin{matrix}-j,0\\0\end{matrix}\right) - \frac{B_g \Gamma(\kappa_{3,\vartheta}) \prod_{\tau=1,\tau\neq\vartheta}^{3} \Gamma(\kappa_{3,\tau}-\kappa_{3,\vartheta})}{\Gamma(\xi^2+1-\kappa_{3,\vartheta})\Gamma(1+\kappa_{3,\vartheta})} \left(\frac{D}{\Psi\overline{\gamma}_2}\right)^{\kappa_{3,\vartheta}} G_{2,1}^{1,2}\left(\frac{1}{\Psi}\middle|\begin{matrix}-j-\kappa_{3,\vartheta},0\\0\end{matrix}\right) \right], \tag{41}$$

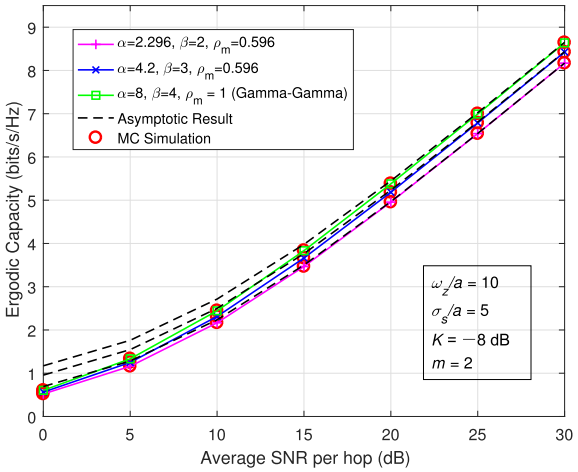

FIGURE 9. Ergodic capacity versus average SNR per hop under weak, moderate and strong turbulence conditions with fixed pointing error effect $\sigma_s/a = 5$.

Figure 8 and 9 illustrate the ergodic capacity of the dual-hop system versus the average SNR per hop under weak, moderate and strong turbulence conditions with varying pointing error effects ($\sigma_s/a = 1$ and $\sigma_s/a = 5$). It is noticeable that when the turbulence strength decreases, the ergodic capacity increases. Moreover, as the pointing error effect increases, the ergodic capacity decreases. When the SNR is large, the asymptotic results are consistent with the exact results as well.

VI. CONCLUSION

In this work, we evaluated the outage probability, the average BERs and the ergodic capacity of the mixed Beaulieu-Xie and $\mathcal{M}$ dual-hop transmission system with digital coherent detection. Novel and exact expressions for the CDF, the PDF and the MGF of the overall SNR were derived by means of Meijer's G function. Capitalizing on these novel results, we further derived the outage probability, average BERs of MPSK and MQAM by means of Meijer's G function, and the ergodic capacity with Meijer's G function as well as EGBMGF. As a special case, the accurate expressions above were derived for the mixed Beaulieu-Xie and Gamma-Gamma dual-hop transmission system as well. Besides, the asymptotic expressions of the CDF, the MGF, the outage probability, the average BERs, and the ergodic capacity were also provided.

Analytical results were presented and verified by MC simulation results. From these results, we find that the turbulence induced fading and zero boresight pointing errors have a strong influence on the system performance. Additionally, the FSO path is dominant between the two hops of the mixed Beaulieu-Xie and $\mathcal{M}$ transmission system.

APPENDIX A
DERIVATION OF THE DIVERSITY ORDER

When the average SNR $\overline{\gamma}$ is large enough, the outage probability can be approximated by [55]

$$P_{\text{out}} \approx (O_c \overline{\gamma})^{-O_d}, \tag{44}$$

where O_c indicates the coding gain, O_d indicates the outage diversity, and $O_d = G_d$.

For the mixed RF/FSO transmission system, the outage probability can be approximated as [27, eq.(58)]

$$\begin{aligned} P_{\text{out}}(\gamma_{\text{th}}) &= F_{\gamma_1}(\gamma_{\text{th}}) + F_{\gamma_2}(\gamma_{\text{th}}) - F_{\gamma_1}(\gamma_{\text{th}}) F_{\gamma_2}(\gamma_{\text{th}}) \\ &\approx F_{\gamma_1}(\gamma_{\text{th}}) + F_{\gamma_2}(\gamma_{\text{th}}). \end{aligned} \tag{45}$$

With the help of [44, eq.(4.63)], $F_{\gamma_1}(\gamma_{\text{th}})$ can be rewritten as

$$\begin{aligned} F_{\gamma_1}(\gamma_{\text{th}}) &= J \exp(-\Psi\gamma_1) \sum_{i=m}^{\infty}\sum_{j=0}^{\infty} \left(\frac{m}{\Omega}\right)^j \frac{\Psi^{i+j}\lambda^{2j}\gamma_{\text{th}}^{i+j}}{j!\Gamma(i+j+1)} \\ &= J \exp\left(-\frac{mA\gamma_{\text{th}}}{\Omega\overline{\gamma}_1}\right) \sum_{i=m}^{\infty}\sum_{j=0}^{\infty} \left(\frac{m}{\Omega}\right)^{i+2j} \\ &\quad \times \frac{\lambda^{2j}A^{i+j}}{j!\Gamma(i+j+1)} \left(\frac{\gamma_{\text{th}}}{\overline{\gamma}_1}\right)^{i+j}. \end{aligned} \tag{46}$$

When $\overline{\gamma}_1 \to \infty$, $\exp\left(-\frac{mA\gamma_{\text{th}}}{\Omega\overline{\gamma}_1}\right) \approx 1 - \frac{mA\gamma_{\text{th}}}{\Omega\overline{\gamma}_1}$, $F_{\gamma_1}(\gamma_{\text{th}})$ can be further rewritten as

$$F_{\gamma_1}(\gamma_{\text{th}}) = \Xi_1 \left(\frac{\gamma_{\text{th}}}{\overline{\gamma}_1}\right)^{i+j} + \Xi_2 \left(\frac{\gamma_{\text{th}}}{\overline{\gamma}_1}\right)^{i+j+1}, \quad i \geq m, j \geq 0, \tag{47}$$

where Ξ_1 and Ξ_2 are constants.

When $\overline{\gamma}_2 \to \infty$, with the help of (11) and [51, eq.(07.34.06.0006.01)], $F_{\gamma_2}(\gamma_{\text{th}})$ can be rewritten as

$$F_{\gamma_2}(\gamma_{\text{th}}) = \Lambda_1 \left(\frac{\gamma_{\text{th}}}{\overline{\gamma}_2}\right)^{\xi^2} + \Lambda_2 \left(\frac{\gamma_{\text{th}}}{\overline{\gamma}_2}\right)^{\alpha} + \Lambda_3 \left(\frac{\gamma_{\text{th}}}{\overline{\gamma}_2}\right)^{k}, \tag{48}$$

where Λ_1, Λ_2 and Λ_3 are constants.

Combining (47) and (48), we can find that the diversity order of the mixed RF/FSO transmission system is relevant to both of the RF path and the FSO path. If $\overline{\gamma}_1 = \overline{\gamma}_2$, the diversity order is $\min\{m, \min\{\xi^2, \alpha, k\}\}$. Similarly, when the FSO link subjects to Gamma-Gamma distributed turbulence, the diversity order can be derived as $\min\{m, \min\{\xi^2, \alpha, \beta\}\}$.

APPENDIX B
DERIVATION OF ASYMPTOTIC EXPRESSIONS FOR THE ERGODIC CAPACITY

According to [54, Representation 2], the EGBMGF in (38) is expressed in terms of the double Mellin-Barnes integral as

$$\begin{aligned} &G_{1,0:2,4:1,1}^{1,0:3,1:1,1}\left(\begin{matrix} j+1 \\ - \end{matrix}\middle|\begin{matrix} 1, \kappa_1 \\ \kappa_2, 0 \end{matrix}\middle|\begin{matrix} 0 \\ 0 \end{matrix}\middle|\begin{matrix} C \\ \Psi\overline{\gamma}_2 \end{matrix}, \frac{1}{\Psi}\right) \\ &= \frac{1}{(2\pi i)^2} \int_{L_1}\int_{L_2} \Gamma(j+1+s+t)\Gamma(s)\Gamma\left(\xi^2 - s\right) \\ &\quad \times \Gamma(\alpha - s)\Gamma(k-s)\Gamma(1+t)\Gamma(-t) \\ &\quad \times \frac{\left(\frac{C}{\Psi\overline{\gamma}_2}\right)^s \left(\frac{1}{\Psi}\right)^t}{\Gamma\left(\xi^2 + 1 - s\right)\Gamma(1+s)} ds dt, \end{aligned} \tag{49}$$

where L_1 and L_2 are integration contours. Equation (49) can be further derived by calculating the residue of the related integrands at the nearest pole to the integration contour [53].

If $\overline{\gamma}_1 \neq \overline{\gamma}_2$, when $\overline{\gamma}_2 \to \infty$, we have $\frac{C}{\Psi\overline{\gamma}_2} \to 0$. The Mellin-Barnes integral over L_1 can be calculated approximately by evaluating the residue at the minimum pole on the right as [56, Theorem 1.11]

$$\begin{aligned}
&\frac{1}{2\pi i}\int_{L_1} \frac{\Gamma(j+1+s+t)\,\Gamma(s)}{\Gamma\left(\xi^2+1-s\right)\Gamma(1+s)} \\
&\quad \underbrace{\times\Gamma\left(\xi^2-s\right)\Gamma(\alpha-s)\,\Gamma(k-s)}_{\upsilon_1(s)}\left(\frac{C}{\Psi\overline{\gamma}_2}\right)^s ds \\
&\approx -\mathrm{Res}\left[\upsilon_1(s), \kappa_{2,\vartheta}\right] \\
&= -\lim_{s\to\kappa_{2,\vartheta}}\left(s-\kappa_{2,\vartheta}\right)\upsilon_1(s) \\
&= \frac{\Gamma\left(j+1+\kappa_{2,\vartheta}+t\right)\Gamma\left(\kappa_{2,\vartheta}\right)\prod_{\tau=1,\tau\neq\vartheta}^{3}\Gamma\left(\kappa_{2,\tau}-\kappa_{2,\vartheta}\right)}{\Gamma\left(\xi^2+1-\kappa_{2,\vartheta}\right)\Gamma\left(1+\kappa_{2,\vartheta}\right)} \\
&\quad \times\left(\frac{C}{\Psi\overline{\gamma}_2}\right)^{\kappa_{2,\vartheta}}, \qquad (50)
\end{aligned}$$

where $\kappa_{2,\vartheta} = \min\left\{\xi^2, \alpha, k\right\}$, and the residue is multiplied by -1 due to a clockwise contour [53]. After substituting the term $\Gamma\left(j+1+\kappa_{2,\vartheta}+t\right)$ in (50) into (49), we get

$$\begin{aligned}
&\frac{1}{2\pi i}\int_{L_2}\Gamma\left(j+1+\kappa_{2,\vartheta}+t\right)\Gamma(1+t)\,\Gamma(-t)\left(\frac{1}{\Psi}\right)^t dt \\
&\qquad = G_{2,1}^{1,2}\left(\frac{1}{\Psi}\middle|\begin{matrix}-j-\kappa_{2,\vartheta}, 0\\ 0\end{matrix}\right). \qquad (51)
\end{aligned}$$

Therefore, we can get (40) by substituting the results of (50) and (51) into (38).

In the case of $\overline{\gamma}_1 = \overline{\gamma}_2$, when $\overline{\gamma}_2 \to \infty$, we have $\frac{1}{\Psi} \to \infty$, and $\frac{C}{\Psi\overline{\gamma}_2}$ is a constant. The Mellin-Barnes integral over L_2 is approximated by evaluating the residue at the maximum pole on the left ($t=-1$) as [56, Theorem 1.7]

$$\begin{aligned}
&\frac{1}{2\pi i}\int_{L_2}\underbrace{\Gamma(j+1+s+t)\,\Gamma(1+t)\,\Gamma(-t)}_{\upsilon_2(t)}\left(\frac{1}{\Psi}\right)^t dt \\
&\approx \mathrm{Res}\left[\upsilon_2(t), -1\right] \\
&= \lim_{t\to-1}(t+1)\,\upsilon_2(t) \\
&= \Psi\Gamma(j+s). \qquad (52)
\end{aligned}$$

Substituting (52) into (49) and employing the definition of Meijer's G function [40, eq.(9.301)], we get

$$\begin{aligned}
&\frac{1}{2\pi i}\int_{L_1}\frac{\Psi\Gamma(j+s)\,\Gamma(s)\,\Gamma\left(\xi^2-s\right)\Gamma(\alpha-s)}{\Gamma\left(\xi^2+1-s\right)\Gamma(1+s)} \\
&\qquad \times\Gamma(k-s)\left(\frac{C}{\Psi\overline{\gamma}_2}\right)^s ds \\
&\quad = \Psi G_{3,4}^{3,2}\left(\frac{C}{\Psi\overline{\gamma}_2}\middle|\begin{matrix}1-j, 1, \kappa_1\\ \kappa_2, 0\end{matrix}\right). \qquad (53)
\end{aligned}$$

When $\frac{1}{\Psi} \to \infty$, $G_{2,1}^{1,2}\left(\frac{1}{\Psi}\middle|\begin{matrix}-j, 0\\ 0\end{matrix}\right)$ in (38) can also be approximated by evaluating the residue at the maximum pole on the left ($s=-1$) as

$$\begin{aligned}
&G_{2,1}^{1,2}\left(\frac{1}{\Psi}\middle|\begin{matrix}-j, 0\\ 0\end{matrix}\right) \\
&\quad = \frac{1}{2\pi i}\int_{L_3}\underbrace{\Gamma(-s)\,\Gamma(1+j+s)\,\Gamma(1+s)}_{\upsilon_3(s)}\left(\frac{1}{\Psi}\right)^s ds \\
&\quad \approx \mathrm{Res}\left[\upsilon_3(s), -1\right] \\
&\quad = \lim_{s\to-1}(s+1)\,\upsilon_3(s) \\
&\quad = \Psi\Gamma(j), \qquad (54)
\end{aligned}$$

where L_3 indicates the integration contour. By substituting (53) and (54) into (38), equation (42) is derived.

Equation (41) and (43) can be derived by using the same method.

REFERENCES

[1] X. Song, F. Yang, J. Cheng, N. Al-Dhahir, and Z. Xu, "Subcarrier phase-shift keying systems with phase errors in lognormal turbulence channels," *J. Lightw. Technol.*, vol. 33, no. 9, pp. 1896–1904, May 1, 2015.
[2] J. Zheng, J. Zhang, S. Chen, H. Zhao, and B. Ai, "Wireless powered UAV relay communications over fluctuating two-ray fading channels," *Phys. Commun.*, vol. 35, Aug. 2019, Art. no. 100724.
[3] M. Safari and M. Uysal, "Relay-assisted free-space optical communication," *IEEE Trans. Wireless Commun.*, vol. 7, no. 12, pp. 5441–5449, Dec. 2008.
[4] M. O. Hasna and M. S. Alouini, "A performance study of dual-hop transmissions with fixed gain relays," *IEEE Trans. Wireless Commun.*, vol. 3, no. 6, pp. 1963–1968, Nov. 2004.
[5] T. Wang, A. Cano, G. B. Giannakis, and J. N. Laneman, "High-performance cooperative demodulation with decode-and-forward relays," *IEEE Trans. Commun.*, vol. 55, no. 7, pp. 1427–1438, Jul. 2007.
[6] J. Zhang, L. Dai, Z. He, B. Ai, and O. A. Dobre, "Mixed-ADC/DAC multipair massive MIMO relaying systems: Performance analysis and power optimization," *IEEE Trans. Commun.*, vol. 67, no. 1, pp. 140–153, Jan. 2019.
[7] J. Zhang, X. Xue, E. Björnson, B. Ai, and S. Jin, "Spectral efficiency of multipair massive MIMO two-way relaying with hardware impairments," *IEEE Wireless Commun. Lett.*, vol. 7, no. 1, pp. 14–17, Feb. 2018.
[8] E. Bjornson, M. Matthaiou, and M. Debbah, "A new look at dual-hop relaying: Performance limits with hardware impairments," *IEEE Trans. Commun.*, vol. 61, no. 11, pp. 4512–4525, Nov. 2013.
[9] G. K. Karagiannidis, T. A. Tsiftsis, and H. G. Sandalidis, "Outage probability of relayed free space optical communication systems," *Electron. Lett.*, vol. 42, no. 17, pp. 994–995, Aug. 2006.
[10] T. A. Tsiftsis, H. G. Sandalidis, G. K. Karagiannidis, and N. C. Sagias, "Multihop free-space optical communications over strong turbulence channels," in *Proc. IEEE Int. Conf. Commun. (ICC)*, vol. 6, Jun. 2006, pp. 2755–2759.
[11] S. Kazemlou, S. Hranilovic, and S. Kumar, "All-optical multihop free-space optical communication systems," *J. Lightw. Technol.*, vol. 29, no. 18, pp. 2663–2669, Sep. 15, 2011.
[12] S. M. Aghajanzadeh and M. Uysal, "Multi-hop coherent free-space optical communications over atmospheric turbulence channels," *IEEE Trans. Commun.*, vol. 59, no. 6, pp. 1657–1663, Jun. 2011.
[13] X. Tang, Z. Wang, Z. Xu, and Z. Ghassemlooy, "Multihop free-space optical communications over turbulence channels with pointing errors using heterodyne detection," *J. Lightw. Technol.*, vol. 32, no. 15, pp. 2597–2604, Aug. 1, 2014.
[14] L. Yang, X. Gao, and M. S. Alouini, "Performance analysis of relay-assisted all-optical FSO networks over strong atmospheric turbulence channels with pointing errors," *J. Lightw. Technol.*, vol. 32, no. 23, pp. 4613–4620, Dec. 1, 2014.
[15] E. Zedini, H. Soury, and M.-S. Alouini, "Dual-hop FSO transmission systems over Gamma–Gamma turbulence with pointing errors," *IEEE Trans. Wireless Commun.*, vol. 16, no. 2, pp. 784–796, Feb. 2017.
[16] E. Lee, J. Park, D. Han, and G. Yoon, "Performance analysis of the asymmetric dual-hop relay transmission with mixed RF/FSO links," *IEEE Photon. Technol. Lett.*, vol. 23, no. 21, pp. 1642–1644, Nov. 1, 2011.

[17] I. S. Ansari, F. Yilmaz, and M.-S. Alouini, "Impact of pointing errors on the performance of mixed RF/FSO dual-hop transmission systems," *IEEE Wireless Commun. Lett.*, vol. 2, no. 3, pp. 351–354, Jun. 2013.

[18] G. T. Djordjevic, M. I. Petkovic, A. M. Cvetkovic, and G. K. Karagiannidis, "Mixed RF/FSO relaying with outdated channel state information," *IEEE J. Sel. Areas Commun.*, vol. 33, no. 9, pp. 1935–1948, Sep. 2015.

[19] H. Samimi and M. Uysal, "End-to-end performance of mixed RF/FSO transmission systems," *IEEE/OSA J. Opt. Commun. Netw.*, vol. 5, no. 11, pp. 1139–1144, Nov. 2013.

[20] E. Zedini, I. S. Ansari, and M.-S. Alouini, "Performance analysis of mixed Nakagami-*m* and Gamma–Gamma dual-hop FSO transmission systems," *IEEE Photon. J.*, vol. 7, no. 1, Feb. 2015, Art. no. 7900120.

[21] L. Kong, W. Xu, L. Hanzo, H. Zhang, and C. Zhao, "Performance of a free-space-optical relay-assisted hybrid RF/FSO system in generalized M-distributed channels," *IEEE Photon. J.*, vol. 7, no. 5, Oct. 2015, Art. no. 7903319.

[22] S. Anees and M. R. Bhatnagar, "Performance of an amplify-and-forward dual-hop asymmetric RF–FSO communication system," *J. Opt. Commun. Netw.*, vol. 7, no. 2, pp. 124–135, Feb. 2015.

[23] L. Yang, M. O. Hasna, and X. Gao, "Performance of mixed RF/FSO with variable gain over generalized atmospheric turbulence channels," *IEEE J. Sel. Areas Commun.*, vol. 33, no. 9, pp. 1913–1924, Sep. 2015.

[24] J. Zhang, L. Dai, Y. Zhang, and Z. Wang, "Unified performance analysis of mixed radio frequency/free-space optical dual-hop transmission systems," *J. Lightw. Technol.*, vol. 33, no. 11, pp. 2286–2293, Jun. 1, 2015.

[25] E. Soleimani-Nasab and M. Uysal, "Generalized performance analysis of mixed RF/FSO cooperative systems," *IEEE Trans. Wireless Commun.*, vol. 15, no. 1, pp. 714–727, Jan. 2016.

[26] P. V. Trinh, T. C. Thang, and A. T. Pham, "Mixed mmWave RF/FSO relaying systems over generalized fading channels with pointing errors," *IEEE Photon. J.*, vol. 9, no. 1, Feb. 2017, Art. no. 5500414.

[27] L. Yang, M. O. Hasna, and I. S. Ansari, "Unified performance analysis for multiuser mixed η-μ and $\mathcal{M}$ - distribution dual-hop RF/FSO systems," *IEEE Trans. Commun.*, vol. 65, no. 8, pp. 3601–3613, Aug. 2017.

[28] J. Gupta, V. K. Dwivedi, and V. Karwal, "On the performance of RF-FSO system over Rayleigh and Kappa-Mu/inverse Gaussian fading environment," *IEEE Access*, vol. 6, pp. 4186–4198, 2018.

[29] N. C. Beaulieu and X. Jiandong, "A novel fading model for channels with multiple dominant specular components," *IEEE Wireless Commun. Lett.*, vol. 4, no. 1, pp. 54–57, Feb. 2015.

[30] A. AlAmmouri, H. ElSawy, A. Sultan-Salem, M. D. Renzo, and M. S. Alouini, "Modeling cellular networks in fading environments with dominant specular components," in *Proc. IEEE Int. Conf. Commun. (ICC)*, May 2016, pp. 1–7.

[31] A. Olutayo, H. Ma, J. Cheng, and J. F. Holzman, "Level crossing rate and average fade duration for the Beaulieu-Xie fading model," *IEEE Wireless Commun. Lett.*, vol. 6, no. 3, pp. 326–329, Jun. 2017.

[32] A. Jurado-Navas, J. M. Garrido-Balsells, J. F. Paris, and A. Puerta-Notario, *A Unifying Statistical Model for Atmospheric Optical Scintillation*. Rijeka, Croatia: InTech, 2011, pp. 181–206.

[33] M. Niu, X. Song, J. Cheng, and J. F. Holzman, "Performance analysis of coherent wireless optical communications with atmospheric turbulence," *Opt. Express*, vol. 20, no. 6, pp. 6515–6520, Mar. 2012.

[34] M. Niu, J. Cheng, and J. F. Holzman, "Error rate performance comparison of coherent and subcarrier intensity modulated optical wireless communications," *IEEE/OSA J. Opt. Commun. Netw.*, vol. 5, no. 6, pp. 554–564, Jun. 2013.

[35] K. Kikuchi, "Fundamentals of coherent optical fiber communications," *J. Lightw. Technol.*, vol. 34, no. 1, pp. 157–179, Jun. 1, 2016.

[36] N. Cvijetic, D. Qian, J. Yu, Y.-K. Huang, and T. Wang, "Polarization-multiplexed optical wireless transmission with coherent detection," *J. Lightw. Technol.*, vol. 28, no. 8, pp. 1218–1227, Apr. 15, 2010.

[37] R. Zhang, J. Wang, G. Zhao, and J. Lv, "Fiber-based free-space optical coherent receiver with vibration compensation mechanism," *Opt. Express*, vol. 21, no. 15, pp. 18434–18441, Jul. 2013.

[38] D. J. Geisler, T. M. Yarnall, M. L. Stevens, C. M. Schieler, B. S. Robinson, and S. A. Hamilton, "Multi-aperture digital coherent combining for free-space optical communication receivers," *Opt. Express*, vol. 24, no. 12, pp. 12661–12671, Jun. 2016.

[39] X. Li, T. Geng, S. Ma, Y. Li, S. Gao, and Z. Wu, "Performance improvement of coherent free-space optical communication with quadrature phase-shift keying modulation using digital phase estimation," *Appl. Opt.*, vol. 56, no. 16, pp. 4695–4701, May 2017.

[40] I. Gradshteyn and I. Ryzhik, *Table of Integrals, Series, and Products*, 7th ed. Boston, MA, USA: Academic, 2007.

[41] B. L. Sharma and R. F. A. Abiodun, "Generating function for generalized function of two variables," *Proc. Amer. Math. Soc.*, vol. 46, no. 1, pp. 69–72, Oct. 1974.

[42] K. Kikuchi and S. Tsukamoto, "Evaluation of sensitivity of the digital coherent receiver," *J. Lightw. Technol.*, vol. 26, no. 13, pp. 1817–1822, Jul. 1, 2008.

[43] M. Niu, J. Cheng, and J. F. Holzman, "Error rate analysis of M-ary coherent free-space optical communication systems with K-distributed turbulence," *IEEE Trans. Commun.*, vol. 59, no. 3, pp. 664–668, Mar. 2011.

[44] M. K. Simon and M. S. Alouini, *Digital Communication over Fading Channels*, 2nd ed. New Jersey, NJ, USA: Wiley, 2005.

[45] M. Abramowitz, *Handbook of Mathematical Functions: With Formulas, Graphs, and Mathematical Tables*. New York, NY, USA: Dover, 1974.

[46] J. Zheng, J. Zhang, G. Pan, J. Cheng, and B. Ai, "Sum of squared fluctuating two-ray random variables with wireless applications," *IEEE Trans. Veh. Technol.*, vol. 68, no. 8, pp. 8173–8177, Aug. 2019.

[47] A. Jurado-Navas, J. M. Garrido-Balsells, J. F. Paris, M. Castillo-Vázquez, and A. Puerta-Notario, "Impact of pointing errors on the performance of generalized atmospheric optical channels," *Opt. Express*, vol. 20, no. 11, pp. 12550–12562, May 2012.

[48] A. A. Farid and S. Hranilovic, "Outage capacity optimization for free-space optical links with pointing errors," *J. Lightw. Technol.*, vol. 25, no. 7, pp. 1702–1710, Jul. 2007.

[49] I. S. Ansari, F. Yilmaz, and M.-S. Alouini, "Performance analysis of free-space optical links over Málaga ($\mathcal{M}$) turbulence channels with pointing errors," *IEEE Trans. Wireless Commun.*, vol. 15, no. 1, pp. 91–102, Jan. 2016.

[50] S. Anees and M. R. Bhatnagar, "Performance evaluation of decode-and-forward dual-hop asymmetric radio frequency-free space optical communication system," *IET Optoelectron.*, vol. 9, no. 5, pp. 232–240, Oct. 2015.

[51] W. Research. (2019). *The Wolfram Functions Site*. [Online]. Available: http://functions.wolfram.com/

[52] V. S. Adamchik and O. I. Marichev, "The algorithm for calculating integrals of hypergeometric type functions and its realization in REDUCE system," in *Proc. Int. Conf. Symbolic Algebr. Comput.*, 1990, pp. 212–224.

[53] H. Chergui, M. Benjillali, and S. Saoudi, "Performance analysis of project-and-forward relaying in mixed MIMO-pinhole and Rayleigh dual-hop channel," *IEEE Commun. Lett.*, vol. 20, no. 3, pp. 610–613, Mar. 2016.

[54] I. S. Ansari, S. Al-Ahmadi, F. Yilmaz, M. S. Alouini, and H. Yanikomeroglu, "A new formula for the BER of binary modulations with dual-branch selection over generalized-K composite fading channels," *IEEE Trans. Commun.*, vol. 59, no. 10, pp. 2654–2658, Oct. 2011.

[55] Z. Wang and G. B. Giannakis, "A simple and general parameterization quantifying performance in fading channels," *IEEE Trans. Commun.*, vol. 51, no. 8, pp. 1389–1398, Aug. 2003.

[56] A. A. Kilbas and M. Saigo, *H-Transforms: Theory and Applications*. Boca Raton, FL, USA: CRC Press, 2004.

JIASHUN HU received the B.S. degree in telecommunications engineering from Sichuan Normal University, Chengdu, China, in 2009, and the M.S. degree in communication and information system from Shenzhen University, Shenzhen, China, in 2012. From May 2017 to September 2018, he was a Visiting International Research Student with the School of Engineering, The University of British Columbia, Okanagan Campus, Kelowna, Canada. He is currently pursuing the Ph.D. degree with the National Mobile Communications Research Laboratory, Southeast University, Nanjing, China. His research interests include digital coherent detection and optical wireless communications.

ZAICHEN ZHANG (SM'15) received the B.S. and M.S. degrees in electrical and information engineering from Southeast University, Nanjing, China, in 1996 and 1999, respectively, and the Ph.D. degree in electrical and electronic engineering from The University of Hong Kong, Hong Kong, in 2002. From 2002 to 2004, he was a Postdoctoral Fellow with the National Mobile Communications Research Laboratory, Southeast University, where he is currently a Professor. He has authored more than 200 articles and issued 30 patents. His current research interests include 6G mobile information systems, optical wireless communications, and quantum information technologies.

JIAN DANG (M'15) received the B.S. degree in information engineering and the Ph.D. degree in information and communications engineering from Southeast University, Nanjing, China, in July 2007 and September 2013. From September 2010 to March 2012, he was a Visiting Scholar with the Department of Electrical and Computer Engineering, University of Florida, Gainesville, FL, USA. Since September 2013, he has been with the National Mobile Communications Research Laboratory, Southeast University, Nanjing, as a Lecturer and an Associate Professor, since 2017. His research interests include signal processing in wireless communications, nonorthogonal multiple access schemes, and optical wireless communications.

LIANG WU (M'13) received the B.S., M.S., and Ph.D. degrees from the School of Information Science and Engineering, Southeast University, Nanjing, China, in 2007, 2010, and 2013, respectively, where he joined the National Mobile Communications Research Laboratory, in September 2013. From September 2011 to March 2013, he was a Visiting Ph.D. Student with the School of Electrical Engineering and Computer Science, Oregon State University. Since April 2018, he has been an Associate Professor with Southeast University. His research interests include optical wireless communications, multiple-input and multiple-output technology, interference alignment, and wireless indoor localization.

GUANGHAO ZHU received the Ph.D. degree in applied physics from the University of Connecticut, Storrs, CT, USA, in 2004. Following six years of postdoctoral training programs at Cornell University, Ithaca, NY, USA, and at the University of California at Los Angeles, CA, USA. He joined Nanjing University, Nanjing, China, as a Faculty Member. His research interests include photonic device design and laser engineering.